CHEMMEDCHEM

ChemPubSoc Europe

DOI: 10.1002/cmdc.201200286

Differentiating between Models of Epothilone Binding to Microtubules Using Tubulin Mutagenesis, Cytotoxicity, and Molecular Modeling

Ruth A. Entwistle,[b] Rania S. Rizk,[a] Daniel M. Cheng,[a] Gerald H. Lushington,[c] Richard H. Himes,[b] and Mohan L. Gupta, Jr.*[a]

Microtubule stabilizers are powerful antimitotic compounds and represent a proven cancer treatment strategy. Several classes of compounds in clinical use or trials, such as the taxanes and epothilones, bind to the same region of β-tubulin. Determining how these molecules interact with tubulin and stabilize microtubules is important both for understanding the mechanism of action and enhancing chemotherapeutic potential, for example, minimizing side effects, increasing solubility, and overcoming resistance. Structural studies using non-polymerized tubulin or stabilized polymers have produced different models of epothilone binding. In this study we used directed mutagenesis of the binding site on *Saccharomyces cerevisiae* β-tubulin to analyze interactions between epothilone B and its biologically relevant substrate, dynamic microtubules. Five engineered amino acid changes contributed to a 125-fold increase in epothilone B cytotoxicity independent of inherent microtubule stability. The mutagenesis of endogenous β-tubulin was done in otherwise isogenic strains. This facilitated the correlation of amino acid substitutions with altered cytotoxicity using molecular mechanics simulations. The results, which are based on the interaction between epothilone B and dynamic microtubules, most strongly support the binding mode determined by NMR spectroscopy-based studies. This work establishes a system for discriminating between potential binding modes and among various compounds and/or analogues using a sensitive biological activity-based readout.

Introduction

Antimitotic compounds that bind tubulin and disrupt microtubule dynamics provide for important cancer therapies, and understanding the molecular mechanisms of these compounds holds the promise of optimizing and exploiting this clinically proven strategy. The taxanes represent an important class of anticancer agents; for example, paclitaxel and docetaxel produce cytotoxicity by enhancing the assembly of tubulin, stabilizing microtubules, suppressing microtubule dynamics, and causing mitotic arrest and apoptosis.[1] The epothilones are a group of natural products produced by the myxobacterium *Sorangium cellulosum*[2] that bind to tubulin in microtubules at a site that overlaps with the paclitaxel site, generating cytotoxicity through a similar mechanism.[3,4] An attractive property of the epothilones is that they may retain excellent activity against cells that have become resistant to the taxanes due to overexpression of the multi-drug transporter.[3–5] Currently epothilone B (EpoB, Figure 1) and various epothilone analogues are in clinical trials,[6] and Ixabepilone is approved for use against some cancers. However, the molecular interactions between the epothilones and tubulin/microtubules remain unclear.

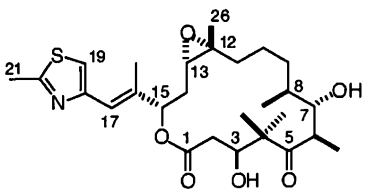

Figure 1. Structure of epothilone B (EpoB).

The region of β-tubulin that binds to the taxanes and epothilones can exert a powerful influence over microtubule dynamics. Moreover, knowledge of the molecular details at this site carries significant clinical potential. Our current understanding of how taxanes and epothilones interact with β-tubulin comes mainly from the electron crystal (EC) structures of complexes between the compounds and a tubulin polymer induced by zinc ions,[7,8] and from NMR spectroscopy,[9,10] supported by structure–activity relationship (SAR) analysis[11] and molecular modeling efforts.[12] Although the two classes of compounds compete with each other for binding[3,4] and bind to the same cavity in β-tubulin,[3,4] the EC structures of the drug–tubulin polymer complexes have shown that the binding interactions are not identical.[7,8] This is also reflected in results

[a] *Dr. R. S. Rizk,[+] D. M. Cheng, Prof. M. L. Gupta, Jr.*
Department of Molecular Genetics and Cell Biology
University of Chicago, Chicago, IL 60637 (USA)
E-mail: mlgupta@uchicago.edu

[b] *Dr. R. A. Entwistle,[+] Prof. R. H. Himes*
Department of Molecular Biosciences
University of Kansas, Lawrence, KS 66045-7534 (USA)

[c] *Dr. G. H. Lushington*
Molecular Graphics and Modeling Laboratory
University of Kansas, Lawrence, KS 66045-7582 (USA)

[+] *These authors contributed equally to this work.*

with wild-type yeast tubulin. EpoB binds to *Saccharomyces cerevisiae* tubulin, but paclitaxel does not.[13]

Two strikingly distinct models of epothilone binding to tubulin have been generated using an NMR-based[10] approach or EC-derived[7] measurements at ~3 Å resolution, which was not adequate to directly define the bound conformation. Thus there is a need to determine the active conformation of tubulin-bound epothilone using structure–activity approaches. To date, SAR data for the epothilones have been limited to ligand binding studies with wild-type tubulin, or spontaneously occurring tubulin mutations in tumor or culture cell lines. Alternatively, site-directed mutagenesis of endogenous tubulin would allow controlled analysis of the epothilone binding pocket. By converting five residues in *S. cerevisiae* β-tubulin to those of mammalian brain tubulin, we were able to impart paclitaxel binding activity to budding yeast tubulin.[14,15] Herein we report that the five amino acid changes that confer paclitaxel binding to yeast tubulin drastically increase the cytotoxicity of EpoB, indicating that the interactions that mediate the potency of both compounds may be more similar than previously predicted based on electron crystallography.[7] These changes, Ala19Lys, Thr23Val, Gly26Asp, Asn227His, and Tyr270Phe allowed the role of each of these residues to be individually examined. This effect was cumulatively mediated by the five substitutions. Thus, we were able to use molecular modeling simulations to distinguish between the current models for the binding of EpoB to tubulin.

Results and Discussion

Mutations in the taxane binding region of β-tubulin mediate EpoB cytotoxicity

We found that changing five residues in the yeast β-tubulin EpoB binding pocket to those found in bovine brain tubulin (Tub2-BBBBB) increased the cytotoxicity of EpoB for these cells 125-fold (Table 1). The ED_{50} value for cells with wild-type tubulin (Tub2-YYYYY) was 2633 nM, whereas Tub2-BBBBB-containing yeast had an ED_{50} of just 21 nM. Thus, some or all of these five substitutions are responsible for optimizing microtubule-stabilizing interactions between EpoB and tubulin.

To hone in on the specific interactions responsible for the cytotoxic effects of EpoB, we created variant tubulins by individually changing the five substitutions in Tub2-BBBBB back to those found in yeast tubulin. These new variants showed a range of sensitivities. Figure 2 represents the growth inhibition by EpoB from a single experiment, while Table 1 lists the results from three to five experiments for each tubulin variant. Compared with Tub2-BBBBB yeast, the greatest losses in cytotoxicity occurred when either the Lys19 or the His227 of brain tubulin was back mutated to the Ala19 or Asn227 of yeast (Tub2-YBBBB or Tub2-BBBYB). These single amino acid changes were each associated with a 13-fold increase in ED_{50} (Table 1). Yeast strains with individual brain-to-yeast back mutations Val23Thr, Asp26Gly, or Phe270Tyr, on the other hand, showed only modest decreases in cytotoxicity. The ED_{50} values of the Thr23, Gly26, or Tyr270 strains increased roughly twofold relative to cells with all five substitutions (50, 46, and 38 nM versus 21 nM, respectively). Thus, Lys19 and His227 contribute significantly to effective interactions between tubulin and EpoB. However, the cumulative effect of the five mutations was much greater than any single mutation.

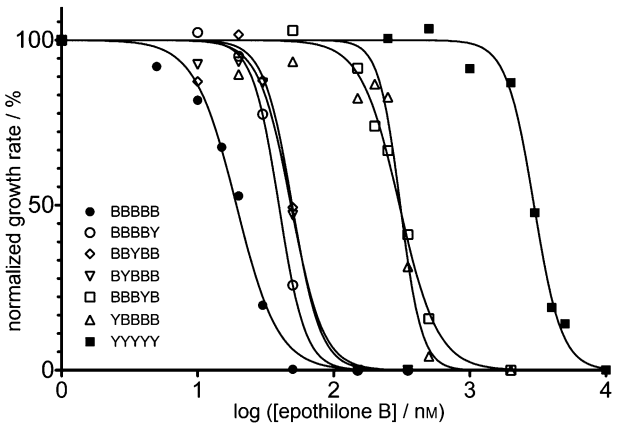

Figure 2. Growth inhibition of *S. cerevisiae* strains with modified β-tubulin by EpoB. The graph depicts a representative experiment in which growth rates were monitored over 24 h in the presence of increasing EpoB concentrations.

Table 1. EpoB ED_{50} values for *S. cerevisiae* strains with modified β-tubulin.

Tubulin form	ED_{50} [nM][a]	ED_{50}(YYYYY)/ED_{50}[b]
Tub2-BBBBB	21 ± 3	125
Tub2-BBBBY	38 ± 8	69
Tub2-BBYBB	46 ± 6	57
Tub2-BYBBB	50 ± 7	53
Tub2-BBBYB	276 ± 50	10
Tub2-YBBBB	277 ± 28	10
Tub2-YYYYY	2633 ± 362	1

[a] The cytotoxicity of epothilone B toward various yeast strains was determined as described in the Experimental Section; values reflect the average ± SEM of three to five experiments. [b] Relative cytotoxicity.

Mutations in the taxane binding region of β-tubulin do not increase inherent microtubule stability

Although all five mutated residues lie within the EpoB binding pocket of tubulin, it is possible that the mutations generally stabilize microtubules, either intrinsically or by disrupting interactions with cellular regulators. This could render cells more sensitive to microtubule stabilizers such as EpoB, resulting in an increase in cytotoxicity. To determine whether the five mutations had stabilized microtubules independently of EpoB binding, we analyzed in vivo microtubule dynamics in cells containing Tub2-YYYYY or Tub2-BBBBB in the absence of EpoB (Figure 3). Overall, we found microtubule dynamics in the two strains to be largely unaffected by the substitutions alone, suggesting the observed cytotoxicity is due to EpoB–tubulin interactions (Table 2). The most notable changes in the Tub2-BBBBB cells were a decrease in depolymerization rate and an increase in attenuation, which could reflect slightly stabilized microtu-

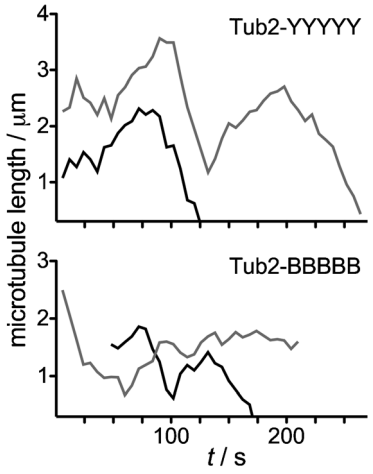

Figure 3. Cytoplasmic microtubule dynamic behavior in G_1 cells containing Tub2-YYYYY (top), and Tub2-BBBBB (bottom). Two representative lifetime history plots (black and grey) depicting the length of individual microtubules over time are presented for each condition.

Table 2. Parameters of dynamic instability for cytoplasmic microtubules in vivo.[a]

Tubulin form	Tub2-BBBBB	Tub2-YYYYY
Polymerization rate [μm min^{-1}]	1.4 ± 0.7 (30)	1.7 ± 0.7 (33)
Depolymerization rate [μm min^{-1}]	1.9 ± 0.7 (38)*	2.6 ± 1.2 (38)
Catastrophe frequency [min^{-1}]	0.59 (28)	0.64 (29)
Rescue frequency [min^{-1}]	1.07 (21)	1.33 (25)
Time spent polymerizing [%]	24	29
Time spent depolymerizing [%]	29	29
Time spent attenuated [%]	46	42
Polymerization duration [s]	33 ± 13 (30)	34 ± 16 (33)
Depolymerization duration [s]	31 ± 15 (38)	30 ± 15 (33)
Attenuation duration [s]	44 ± 28 (44)*	34 ± 16 (49)
Total microtubules observed	28	28
Total time observed [s]	4014	3858

[a] Number of events is given in parentheses; rates and durations are listed as the mean value ± SD; *$p < 0.05$ relative to Tub2-YYYYY as determined by unpaired two-tailed *t*-test.

bules. However, this was accompanied by a decrease in rescue frequency relative to Tub2-YYYYY cells, which may reflect slightly destabilized microtubules.

For inherent microtubule stability to be responsible for the graded cytotoxicity profile, each mutation would likely contribute some degree of increased microtubule stability. Previously, of 53 mutations created in an alanine-scanning analysis of yeast Tub1 (α-tubulin), only six (11%) produced detectable levels of resistance to the microtubule-destabilizing compound benomyl, suggestive of microtubule stabilization.[16] However, 37 mutations (70%) increased sensitivity to benomyl, revealing that overall, tubulin mutations are more likely to destabilize rather than stabilize microtubules. Likewise, in our previous systematic analysis of cysteine residues in Tub2, 17% of mutations resulted in increased benomyl resistance, whereas 42% caused increased benomyl sensitivity.[17] These results support our conclusion that the increased EpoB cytotoxicity is directly due to increased affinity of the drug for the mutated tubulins.

Molecular modeling correlates amino acid changes with EpoB cytotoxicity

Together, our cytotoxicity results and microtubule dynamics comparison demonstrate that the five mutated residues differentially contribute to the binding affinity of EpoB for tubulin and/or microtubules. To help interpret the changes in the EpoB ED_{50} values as a function of the different binding site mutations, we performed molecular mechanics simulations based on the EC and NMR structures using a yeast tubulin homology model. The binding scores for EpoB interacting with the panel of tubulin mutants, presented in Table 3, were determined by using four different formulations: ChemScore,[18] DrugScore,[19] G-Score,[20] and PMF.[21] The various scoring models generate different quantitative values because each takes into account a different set of physicochemical properties. Therefore, scores for different mutants within a given formulation can be compared in order to understand the relative contribution of each residue to EpoB binding. Also, this allows correlation of the scores of each mutation in the EC and NMR models with the observed in vivo cytotoxicity data.

The scores for both models largely predicted Tub2-YYYYY to exhibit the lowest affinity for EpoB, while the bovine-like Tub2-BBBBB produced the highest ligand affinity. Additionally, the scores for Tub2-YBBBB, the mutant with the lowest sensitivity, strikingly discriminated between the EC and NMR binding modes across all four scoring models (Table 3, bold text). In the EC model the scores for this mutant were close to those for Tub2-BBBBB and ranged from the first to fourth highest ligand affinities of the tubulin variants containing four of the five brain residues. Conversely, in the NMR model the values were much closer to those for Tub2-YYYYY, and always predicted the lowest EpoB binding affinity of the six tubulin mutants. Clearly, the NMR model more correctly predicted the cytotoxicity data for Tub2-YBBBB.

In both models the scores for Tub2-BBBBY, Tub2-BBYBB, and Tub2-BYBBB correlated well with the cytotoxicity data. The scores were closer to those for Tub2-BBBBB than to Tub2-YYYYY. Also consistent with the cytotoxicity data is the fact that the scores for Tub2-BBBYB were farther away from Tub2-BBBBB, and fell somewhere between the scores for Tub2-BBBBB and Tub2-YYYYY. Of the two models, the binding scores produced by the NMR model generally correlated better with the in vivo cytotoxicity data across the range of tubulin variants (Table 3).

Variations in the predicted binding mode as a function of different tubulin mutants are reported in Figure 4 for models assessed from NMR data (upper two quadrants) and EC characterization (lower). These illustrations each focus on comparing the most potent complex (EpoB bound to Tub2-BBBBB) with those of two specific tubulin variants: Tub2-YBBBB (left side) and Tub2-BBBYB (right side). From these figures, one can per-

Table 3. Approximate binding scores computed for EpoB in complex with mutants of yeast tubulin as a function of binding mode model and computational scoring function.[a]

Tubulin form	EC model[b]				NMR model[c]			
	Chem[d]	Drug[e]	G[f]	PMF[g]	Chem	Drug	G	PMF
Tub2-BBBBB	−23.14	−100.8	−195.0	−40.49	−22.43	−113.4	−181.6	−33.00
Tub2-BBBBY	−23.02	−101.9	−194.8	−36.79	−21.62	−111.0	−176.8	−27.03
Tub2-BBYBB	−22.66	−97.7	−193.8	−38.96	−21.90	−108.6	−177.1	−32.95
Tub2-BYBBB	−22.11	−100.5	−197.4	−36.48	−20.97	−111.9	−177.2	−36.21
Tub2-BBBYB	−19.55	−87.5	−165.6	−27.56	−19.19	−102.4	−160.4	−18.96
Tub2-YBBBB	**−22.60**	**−99.7**	**−188.3**	**−39.65**	**−16.80**	**−96.2**	**−139.7**	**−11.36**
Tub2-YYYYY	−10.72	−83.8	−126.4	−17.00	−14.20	−93.9	−145.9	−11.11
Correlation $R(\log[ED_{50}])$	0.75	0.51	0.73	0.68	0.83	0.76	0.70	0.77

[a] Different scoring functions have different physical interpretations, but in each case a more negative score indicates stronger binding, and in each case, as shown in the bottom row, scores should roughly correlate with $\log[ED_{50}]$. [b] Ref. [7]. [c] Ref. [10]. [d] ChemScore.[18] [e] DrugScore.[19] [f] G-Score.[20] [g] PMF.[21]

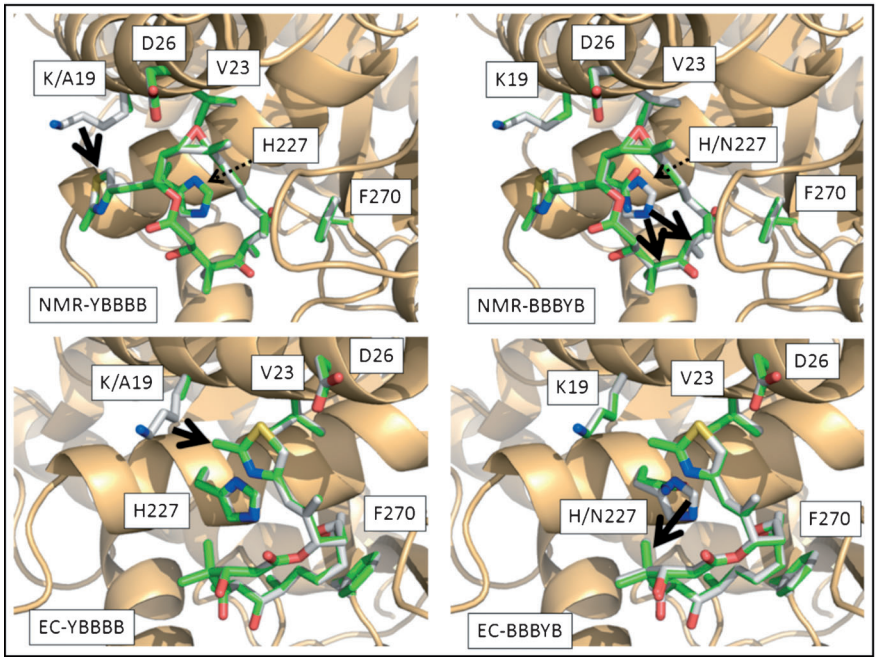

Figure 4. Comparisons between the computationally minimized structures for the complex of EpoB bound to Tub2-BBBBB tubulin (grey structures in all panels) versus EpoB in complex with the Tub2-YBBBB (left-hand quadrants) or Tub2-BBBYB (right quadrants) tubulin mutants (shown as green-colored sticks in all panels). The two top quadrants depict complexes solved based on ligand binding according to NMR characterization,[10] while the two bottom quadrants depict complexes derived from assuming binding modes analogous to the EC prediction.[7] All heteroatoms within the ligand (EpoB) and key receptor residues (tubulin) are colored according to standard CPK coloring; tubulin secondary structure is rendered as tan ribbons. Thick black arrows denote favorable interactions in the Tub2-BBBBB complex which are absent for corresponding mutants. Thin dashed arrows indicate the position of residue 227.

ceive clear differences in the predicted EpoB binding modes arising from the NMR and EC models; however, there are also similarities across the two models in the *types* of EpoB–tubulin interactions that are predicted to occur.

The fairly benign nature of the back-substitutions at residues 23, 26, and 270 can be explained by the following analysis. In both the NMR and EC models, the side chain methyl groups of Val23 (Tub2-BBBBB) engage in favorable lipophilic interactions with EpoB that are not fully matched by Thr23 (Tub2-BYBBB). In the NMR structure, both methyl carbons on Val23 of Tub2-BBBBB are predicted to have lipophilic interactions with 11-methylene on EpoB (4.03 and 4.15 Å, respectively), whereas for Tub2-BYBBB, Thr23 has only one side chain methyl (at a distance of 4.05 Å) to produce a similar interaction. In the EC model, whereas both of the Val23 methyl groups have modest interactions with EpoB (one with the 21-methyl at 4.20 Å; the other with 26-methyl at 4.58 Å), Thr23 appears to engage in no favorable lipophilic interactions, instead only forming a possible weak hydrogen bond between the side chain hydroxy group proton and the thiazole nitrogen atom of EpoB (3.77 Å). In the EC and NMR models, the Asp26 Cα in Tub2-BBBBB approaches somewhat more closely to favorable lipophilic contacts than does Gly26 Cα in Tub2-BBYBB (4.63 versus 4.92 Å separation from the thiazole in the EC model; 4.90 versus 5.13 Å distance from 12-methyl for the NMR complex). Furthermore, the Asp26 Cβ (not present in Tub2-BBYBB) is also available for weak lipophilic interactions in both models. The structure of the Tub2-BBBBY (Tyr270) complex with EpoB is very similar to that observed for Tub2-BBBBB (Phe270) in both models; however, the very modest difference in EpoB potency upon mutation of this residue can be rationalized by slightly closer proximity between Phe270 and EpoB carbon atoms (EC: 3.91 Å; NMR: 3.73 Å) than is possible for Tyr270 (EC: 4.18 Å; NMR: 3.84 Å), with all other aspects of the complexes being very closely conserved upon mutation. Together the modeling and cytotoxicity data suggest that Phe270 does not mediate critical interactions with EpoB. Consistent with this conclusion, a human ovarian carcinoma cell line with an acquired Phe270Val mutation displayed 24-fold paclitaxel resistance, yet only a threefold effect on EpoB activity.[22]

The predicted structure for the epothilone binding site in the yeast tubulin homology model is marginally more spatially constricted than that resolved for bovine brain tubulin. Thus, whereas prior studies have suggested close interactions between the EpoB thiazole ring and the His227 residue in bovine brain tubulin,[7,10,13] such coupling may not be energetically favored in the more constrained yeast tubulin receptor. Specifically, for a receptor model based on the yeast tubulin sequence, we do not predict that the EpoB thiazole ring will engage in hydrogen bonding with the Asn227 residue present in wild-type yeast tubulin or in either hydrogen bonding or π-stacking with His227 present in the mutant forms. Rather, both the EC and NMR models predict lipophilic interactions between the imidazole ring of His227 and the EpoB macrocycle. In the EC model there is a 3.57 Å separation between the imidazole ring and the 4-methyl on EpoB for Tub2-BBBBB, and in the NMR model there is a 3.81 and 3.96 Å distance to the 4-methyl and 6-methyl, respectively. The lipophilic interactions between the imidazole ring and the EpoB 4- or 6-methyls are unavailable to the Asn227 residue in Tub2-BBBYB. An additional difference evident in the NMR model is further EpoB stabilization by His (as compared with Asn) via a methyl–π interaction with EpoB 16-methyl (3.21 Å separation).

Ala19 in Tub2-YBBBB does not have significant interactions with EpoB in either the NMR or EC models; however, the mutation to Lys19 affords favorable lipophilic contact in both cases. Specifically, in the case of the EC model, the methyl carbon located off the thiazole ring approaches within 4.39 Å of Cγ on the Lys19 side chain, while in the NMR model, the unsubstituted thiazole carbon is within 3.83 Å of Lys19 Cγ. In the latter case, there may also be a modest electrostatic coupling between the lysine cationic nitrogen and the thiazole sulfur atom (4.22 Å separation).

From this analysis, it is apparent that both the NMR and EC models predict that similarly favorable interactions, between EpoB and its high-potency complex with Tub2-BBBBB, are disrupted in the various back-mutational forms and the low potency Tub2-YYYYY receptor. This is likely the reason that both the EC and NMR models produced consistently high levels of correlation between computed binding scores and experimentally observed ED_{50} data (Table 3). While the predicted models we have generated herein do not lend definitive corroboration to the NMR relative to the EC model, the NMR model better explains the cytotoxicity results of the Tub2-YBBBB mutant and produced higher correlations with observed in vivo results.

Summary

Determining the biologically relevant interactions between the taxanes/epothilones and microtubules is an important goal. Current models of these interactions are based largely on artificial systems (non-polymerized tubulin[9,10] and zinc-stabilized tubulin sheets).[7,8] Using in vivo microtubules as substrates we demonstrated that amino acids critical for paclitaxel binding also strongly promote the cytotoxicity of EpoB, indicating that similar interactions may mediate the toxicity of both compounds. However, the three substitutions that were most critical for paclitaxel activity were least important for EpoB activity (Thr23Val, Gly26Asp, Try270Phe), while the two substitutions dispensable to paclitaxel activity made the largest contributions to EpoB activity (Ala19Lys, Asn227His).[23] Interestingly, this trend illustrates that there are also fundamental differences in the binding interactions of the two compounds. Paclitaxel and EpoB have been shown to stimulate the in vitro assembly of Tub2-BBBBB with similar activities.[14] Therefore, it is interesting that yeast containing the modified tubulin were ~300-fold more sensitive to EpoB than reported for paclitaxel: 21 versus 6500 nM,[23] respectively. Similar differences in human cells result from inefficient export of EpoB by the ABC-transport protein P-glycoprotein.[3] Correspondingly, perhaps paclitaxel, and not EpoB, is a substrate for any transport activity remaining in the drug-sensitized AD1-8 yeast strain.

Sub-stoichiometric concentrations of both microtubule stabilizers[24] and inhibitors[25] are known to suppress microtubule dynamics and stabilize the polymer, highlighting the importance of understanding their interactions with dynamic microtubules. Moreover, assays using microtubule substrates in isogenic cells expressing endogenous levels of tubulin will reflect important transitional conformations or specific interactions that may occur at the ends of dynamic microtubules. Site-directed mutagenesis of the taxane/epothilone binding pocket will likely reveal interactions critical to the active conformation and biological activity of these important classes of compounds.

Experimental Section

Yeast strains and cytotoxicity: Yeast growth, genetic manipulations, and lithium acetate transformation were performed using standard techniques.[26] Yeast strains used or created in this study are listed in Table 4.

Table 4. Yeast strains used in this study.

Strain	Relevant genotype
AD1-8[27]	*MAT*a, *PDR1-3*, *ura3*, *his1*, D*yor1::hisG*, D*snq2::hisG*, D*pdr5::hisG*, D*pdr10::hisG*, D*pdr11::hisG*, D*ycf1::hisG*, D*pdr3::hisG*, D*pdr15::hisG*
MGY612	*tub2-YYYYY-His$_6$-URA3*, otherwise isogenic to AD1-8
MGY613	*tub2-BBBBB-His$_6$-URA3*, otherwise isogenic to AD1-8
MGY614	*tub2-BBBBY-His$_6$-URA3*, otherwise isogenic to AD1-8
MGY615	*tub2-BBBYB-His$_6$-URA3*, otherwise isogenic to AD1-8
MGY616	*tub2-BBYBB-His$_6$-URA3*, otherwise isogenic to AD1-8
MGY617	*tub2-BYBBB-His$_6$-URA3*, otherwise isogenic to AD1-8
MGY618	*tub2-YBBBB-His$_6$-URA3*, otherwise isogenic to AD1-8
MGY981	*MAT*a, *tub2-YYYYY-His$_6$-URA3*, *LEU2::GFP-TUB1::leu2*D1
MGY982	*MAT*a, *tub2-BBBBB-His$_6$-URA3*, *LEU2::GFP-TUB1::leu2*D1

To determine the in vivo efficacy of EpoB, the *Saccharomyces cerevisiae* strain AD12345678 (AD1-8),[27] which is deficient in seven drug transporters as well as one transcription factor (*pdr3*), was transformed with a yeast genomic DNA fragment containing the β-tubulin (*TUB2*) coding sequence with different subsets of the five amino acid changes and a C-terminal His_6 tag as previously described (Table 5).[15,17] This transformation strategy replaced the endogenous β-tubulin locus with the mutated version. The sensitivity

Table 5. Specific mutations introduced to the epothilone binding pocket of yeast β-tubulin Tub2.

Tubulin form	Specific mutations
Tub2-BBBBB	A19K, T23V, G26D, N227H, Y270F, C-term His_6
Tub2-BBBBY	A19K, T23V, G26D, N227H, C-term His_6
Tub2-BBBYB	A19K, T23V, G26D, Y270F, C-term His_6
Tub2-BBYBB	A19K, T23V, N227H, Y270F, C-term His_6
Tub2-BYBBB	A19K, G26D, N227H, Y270F, C-term His_6
Tub2-YBBBB	T23V, G26D, N227H, Y270F, C-term His_6
Tub2-YYYYY	C-term His_6

of each strain to EpoB was measured by comparing the growth of an equal number of cells after 24–27 h in rich media (YPD) at 30 °C,[15,23] or by determining the doubling time from the increase in OD_{600} measured every 15 min in a Tecan Safire II plate reader maintained at 30 °C with continuous orbital mixing. The concentration of EpoB that inhibited growth rate by 50% (ED_{50}) was determined from fitting log[EpoB] versus normalized growth rates by nonlinear regression using Prism software (GraphPad).

Fluorescence microscopy and microtubule dynamics analysis: In vivo analyses of microtubule dynamics in G_1 (unbudded) cells were performed essentially as described previously.[28] A control cell harboring an exogenous copy of GFP-Tub1 (α-tubulin; pMG3)[28] under the *TUB1* promoter was then transformed with fragments to replace the endogenous *TUB2* locus with either *tub2-YYYYY-His$_6$* or *tub2-BBBBB-His$_6$* (Table 5). Cells were grown to mid-log phase in SD-complete media (0.67% yeast nitrogen base without amino acids, 2% glucose, and supplemented with amino acids)[26] and placed onto a microscope slide padded with 1% agarose in the same medium. Coverslips were sealed using VALAP and epifluorescence time-lapse images of G_1 cells were obtained on a Zeiss AxioImager M2 microscope with a piezoelectric driven *Z*-stage, 63× 1.4 NA objective, Semrock filters, and a Coolsnap HQ^2 CCD camera (Photometrics Inc.) driven by SlideBook software. Image series consisted of 8–10 *Z*-planes spaced 0.75 μm apart obtained every 6 s for at least 6 min. The three-dimensional length of individual astral microtubules was subsequently determined at each timepoint by using SlideBook software. Polymerization and depolymerization events were defined as a line through at least four data points (24 s) that spanned a range of >0.4 μm with an R^2 value of ≥ 0.84. Periods of attenuation were defined as persisting at least four data points with net length changes of $< \pm 0.2$ μm. Data points that did not fit these criteria were discarded. The percentage of time spent in each phase was determined by dividing the sum of the time in each phase by the total classified time for all microtubules analyzed. Catastrophes were defined as a transition into depolymerization following polymerization or attenuation. Rescues were defined as transition out of depolymerization into polymerization or attenuation. Only the time spent polymerizing or attenuated was considered to determine the catastrophe frequency. Similarly, only time spent depolymerizing was considered to calculate rescue frequency. Cells containing Tub2-YYYYY-His_6 or Tub2-BBBBB-His_6 (MGY981 or MGY982) were imaged on three separate days. Cells were grown and maintained at 23 °C during imaging; *p* values were determined by Student's *t*-test.

Molecular modeling: Molecular mechanics simulations were based on a model of the structure of yeast β-tubulin generated via the SwissModel[29] tool (according to default first-approach mode specifications) based on the epothilone A–bovine brain tubulin electron diffraction crystal structure.[7] Recognizing uncertainty in the real epothilone binding mode, we modeled one scenario that assumed an EpoB binding mode as represented in the original crystallographic structure and a second scenario designed to emulate the binding mode obtained by NMR experiments of Carlomagno et al.[10] To prepare an EpoB–tubulin structure for evaluating the effect of receptor mutations within the context of the original crystal structure, we used SYBYL 8.1 (2009, Tripos Inc., St. Louis, MO, USA) to modify the co-crystallized epothilone A into EpoB (i.e., by substituting a methyl group for the proton on C12 of epothilone A), and created estimated structures for the relevant mutants by substituting the corresponding amino acids (Ala/Lys19, Thr/Val23, Gly/Asp26, Asn/His227, and Phe/Tyr270) via the Biopolymer module in SYBYL. We constructed initial models representing the NMR-predicted scenario in a similar manner, with the exception that we modified the α–β–γ–δ torsion of His227 from 172.2° to 267.6° to support a potential π-stacking interaction with the EpoB thiazole (instead of the previously assumed hydrogen bond), and we repositioned the ligand to encourage lipophilic interactions between the EpoB 4-methyl groups and tubulin residues Leu215, Leu228 and Leu273, and between the 6-methyl group and Ala231 and Phe270. This repositioning was accomplished by a short (1 ps) low-temperature (200 K) molecular dynamics simulation in SYBYL via the Tripos molecular force field[30] and Gasteiger–Marsili electrostatics[31] using weak (10 kcal mol^{-1} Å) constraints that held the interacting carbon pairs (as mentioned above) within 3–5 Å of each other. Together the seven tubulin variants (Tub2-BBBBB, Tub2-YBBBB, Tub2-BYBBB, Tub2-BBYBB, Tub2-BBBYB, Tub2-BBBBY, and Tub2-YYYYY) and two EpoB binding modes produced 14 EpoB–tubulin models.

To gauge the structural effects of each tubulin mutation on the EpoB binding modes, we subjected each of the initial EpoB–tubulin models to molecular mechanics optimization. For each complex, we permitted an unlimited number of optimization steps, employed very fine criteria [maximum displacement of 0.001 Å; maximum ΔE of 0.0005 kcal mol^{-1}; gradient of 0.005 kcal (mol^{-1} Å)], and requested gradient recomputation after every geometry step. To achieve these convergence criteria in a reasonable time, we assumed that the mutations would have only a modest effect on the crystallographically resolved atomic coordinates of conserved residues and thus relaxed only the ligand, plus residues 19, 23, 26, 227, and 270. Based on results from our prior study on paclitaxel interacting with mutations of β-tubulin,[23] we chose to compare computational estimates for the relative EpoB potency in these different receptors via the ChemScore,[18] DrugScore,[19] G-Score[20] and PMF[21] formalisms for estimating the binding score.

Acknowledgements

We thank Travis Foland for excellent technical assistance. R.S.R. was supported by a National Institutes of Health postdoctoral training fellowship (T32HL094282). This work was funded by: a National Institutes of Health grant CA105305 to R.H.H., a National Center for Research Resources (Kansas IDeA Network for Biomedical Research Excellence; NCRR award no. P20RR016475) grant to G.H.L., and a National Institutes of Health grant (R01GM094313), Cancer Research Foundation Young Investigator Grant, and an American Cancer Society Institutional Research Grant (no. IRG-58-004-48) to M.L.G.

Keywords: antitumor agents · drug design · epothilones · microtubules · tubulin

[1] M. A. Jordan, *Curr. Med. Chem. Anticancer Agents* **2002**, *2*, 1 – 17.
[2] K. Gerth, N. Bedorf, G. Hofle, H. Irschik, H. Reichenbach, *J. Antibiot.* **1996**, *49*, 560 – 563.
[3] R. J. Kowalski, P. Giannakakou, E. Hamel, *J. Biol. Chem.* **1997**, *272*, 2534 – 2541.
[4] D. M. Bollag, P. A. McQueney, J. Zhu, O. Hensens, L. Koupal, J. Liesch, M. Goetz, E. Lazarides, C. M. Woods, *Cancer Res.* **1995**, *55*, 2325 – 2333.
[5] a) K. H. Altmann, M. Wartmann, T. O'Reilly, *Biochim. Biophys. Acta Rev. Cancer* **2000**, *1470*, M79 – M91; b) T. O'Reilly, M. Wartmann, J. Brueggen, P. R. Allegrini, A. Floersheimer, M. Maira, P. M. McSheehy, *Cancer Chemother. Pharmacol.* **2008**, *62*, 1045 – 1054.
[6] a) B. Melichar, E. Casado, J. Bridgewater, J. Bennouna, M. Campone, P. Vitek, J. P. Delord, J. Cerman, Jr., R. Salazar, J. Dvorak, C. Sguotti, P. Urban, K. Viraswami-Appanna, E. Tan, J. Tabernero, *Br. J. Cancer* **2011**, *105*, 1646 – 1653; b) B. Bystricky, I. Chau, *Expert Opin. Invest. Drugs* **2011**, *20*, 107 – 117; c) G. Ferrandina, M. Mariani, M. Andreoli, S. Shahabi, G. Scambia, C. Ferlini, *Curr. Pharm. Des.* **2012**, *18*, 2793 – 2803; d) J. J. Lee, S. M. Swain, *Clin. Cancer Res.* **2008**, *14*, 1618 – 1624.
[7] J. H. Nettles, H. Li, B. Cornett, J. M. Krahn, J. P. Snyder, K. H. Downing, *Science* **2004**, *305*, 866 – 869.
[8] J. P. Snyder, J. H. Nettles, B. Cornett, K. H. Downing, E. Nogales, *Proc. Natl. Acad. Sci. USA* **2001**, *98*, 5312 – 5316.
[9] A. Kumar, H. Heise, M. J. Blommers, P. Krastel, E. Schmitt, F. Petersen, S. Jeganathan, E. M. Mandelkow, T. Carlomagno, C. Griesinger, M. Baldus, *Angew. Chem.* **2010**, *122*, 7666 – 7669; *Angew. Chem. Int. Ed.* **2010**, *49*, 7504 – 7507.
[10] T. Carlomagno, M. J. Blommers, J. Meiler, W. Jahnke, T. Schupp, F. Petersen, D. Schinzer, K. H. Altmann, C. Griesinger, *Angew. Chem.* **2003**, *115*, 2615 – 2619; *Angew. Chem. Int. Ed.* **2003**, *42*, 2511 – 2515.
[11] M. Reese, V. M. Sanchez-Pedregal, K. Kubicek, J. Meiler, M. J. Blommers, C. Griesinger, T. Carlomagno, *Angew. Chem.* **2007**, *119*, 1896 – 1900; *Angew. Chem. Int. Ed.* **2007**, *46*, 1864 – 1868.
[12] P. Giannakakou, R. Gussio, E. Nogales, K. H. Downing, D. Zaharevitz, B. Bollbuck, G. Poy, D. Sackett, K. C. Nicolaou, T. Fojo, *Proc. Natl. Acad. Sci. USA* **2000**, *97*, 2904 – 2909.
[13] C. J. Bode, M. L. Gupta, Jr., E. A. Reiff, K. A. Suprenant, G. I. Georg, R. H. Himes, *Biochemistry* **2002**, *41*, 3870 – 3874.
[14] M. L. Gupta, Jr., C. J. Bode, G. I. Georg, R. H. Himes, *Proc. Natl. Acad. Sci. USA* **2003**, *100*, 6394 – 6397.
[15] T. B. Foland, W. L. Dentler, K. A. Suprenant, M. L. Gupta, Jr., R. H. Himes, *Yeast* **2005**, *22*, 971 – 978.
[16] K. L. Richards, K. R. Anders, E. Nogales, K. Schwartz, K. H. Downing, D. Botstein, *Mol. Biol. Cell* **2000**, *11*, 1887 – 1903.
[17] M. L. Gupta, Jr., C. J. Bode, C. A. Dougherty, R. T. Marquez, R. H. Himes, *Cell Motil. Cytoskeleton* **2001**, *49*, 67 – 77.
[18] M. D. Eldridge, C. W. Murray, T. R. Auton, G. V. Paolini, R. P. Mee, *J. Comput. Aided Mol. Des.* **1997**, *11*, 425 – 445.
[19] H. F. Velec, H. Gohlke, G. Klebe, *J. Med. Chem.* **2005**, *48*, 6296 – 6303.
[20] G. Jones, P. Willett, R. C. Glen, *J. Mol. Biol.* **1995**, *245*, 43 – 53.
[21] I. Muegge, Y. C. Martin, P. J. Hajduk, S. W. Fesik, *J. Med. Chem.* **1999**, *42*, 2498 – 2503.
[22] P. Giannakakou, D. L. Sackett, Y. K. Kang, Z. Zhan, J. T. Buters, T. Fojo, M. S. Poruchynsky, *J. Biol. Chem.* **1997**, *272*, 17118 – 17125.
[23] R. A. Entwistle, R. D. Winefield, T. B. Foland, G. H. Lushington, R. H. Himes, *FEBS Lett.* **2008**, *582*, 2467 – 2470.
[24] a) M. A. Jordan, R. J. Toso, D. Thrower, L. Wilson, *Proc. Natl. Acad. Sci. USA* **1993**, *90*, 9552 – 9556; b) W. B. Derry, L. Wilson, M. A. Jordan, *Biochemistry* **1995**, *34*, 2203 – 2211.
[25] K. Gupta, J. Bishop, A. Peck, J. Brown, L. Wilson, D. Panda, *Biochemistry* **2004**, *43*, 6645 – 6655.
[26] *Methods in Enzymology: Guide to Yeast Genetics and Molecular Biology, Vol. 194*, (Eds.: C. Guthrie, G. Fink), Academic Press, **1991**.
[27] A. Decottignies, A. M. Grant, J. W. Nichols, H. de Wet, D. B. McIntosh, A. Goffeau, *J. Biol. Chem.* **1998**, *273*, 12612 – 12622.
[28] M. L. Gupta, Jr., C. J. Bode, D. A. Thrower, C. G. Pearson, K. A. Suprenant, K. S. Bloom, R. H. Himes, *Mol. Biol. Cell* **2002**, *13*, 2919 – 2932.
[29] K. Arnold, L. Bordoli, J. Kopp, T. Schwede, *Bioinformatics* **2006**, *22*, 195 – 201.
[30] M. Clark, R. D. Cramer III, N. van Opdenhosch, *J. Comput. Chem.* **1989**, *10*, 982 – 1012.
[31] J. Gasteiger, M. Marsili, *Tetrahedron Lett.* **1978**, *19*, 3181 – 3184.

Received: June 6, 2012
Published online on July 16, 2012

